Extracellular Processing of Molecular Gradients by Eukaryotic Cells Can Improve Gradient Detection Accuracy

Igor Segota* and Carl Franck
Laboratory of Atomic and Solid State Physics, Cornell University, Ithaca 14853, USA
(Received 26 February 2017; revised manuscript received 2 October 2017; published 14 December 2017)

Eukaryotic cells sense molecular gradients by measuring spatial concentration variation through the difference in the number of occupied receptors to which molecules can bind. They also secrete enzymes that degrade these molecules, and it is presently not well understood how this affects the local gradient perceived by cells. Numerical and analytical results show that these enzymes can substantially increase the signal-to-noise ratio of the receptor difference and allow cells to respond to a much broader range of molecular concentrations and gradients than they would without these enzymes.

DOI: 10.1103/PhysRevLett.119.248101

Eukaryotic cells sense and follow molecular concentration gradients in a process called chemotaxis. This process is essential for numerous biological functions such as proliferation, organ formation, wiring of the nervous system, wound healing, and cancer [1–3]. In contrast to bacteria [4], eukaryotic cells are large enough ($\gtrsim 10$ μm) to be able to directly measure concentration differences across their bodies [5]. This is achieved by taking snapshots of the nonuniform occupancy of their cell surface receptors to which diffusing molecules can bind.

The physical limits of chemotactic sensitivity in eukaryotic cells have been extensively studied both theoretically and experimentally, often by calculating theoretical limits and comparing the accuracy of the experimental chemotaxis response to these limits [5–16].

However, many cells secrete enzymes that can inactivate chemotactic signals, so the local gradient perceived by cells may differ from the applied gradient. For example, *Dictyostelium discoideum* cells secrete phosphodiesterases (PDEs) [17] that inactivate cyclic adenosine monophosphate (cAMP) signals [18], *Saccharomyces cerevisiae* cells secrete Bar1 protease that degrades α-factor pheromone [19–21] and neutrophils can inactivate chemotactic formylmethionyl peptides [3]. The PDEs can help avoid receptor saturation at high cAMP concentrations in *D. discoideum* with many cells present, but it has been suggested that it can also steepen cAMP gradients ([18], p. 125) prevent cells from sensing their own cAMP at low cAMP concentrations [22] and extend the range and robustness of chemotaxis [23]. Similarly, Bar1 has been suggested to improve the detection of the direction of the nearest mating partner in *S. cerevisiae* [19–21].

In *D. discoideum*, PDE exists in both membrane bound and as a secreted extracellular form [17,24–26], both encoded by the same gene *pdsA*. Nanjundiah and Malchow [27] argued, using dimensional analysis, that the extracellular PDE has no observed effect. More recently, Palsson *et al.* [28–30] argued that PDE may be important for the wave propagation at low cell densities. Experimentally, *D. discoideum pdsA*-strain (deleted PDE gene) has been shown to fail to aggregate [31,32] and to respond to a reduced range of cAMP concentrations compared to the wild type [22]. Despite these efforts, it remains poorly understood how extracellular PDE affects the local cAMP gradient perceived by cells.

We address this question by calculating cAMP concentration across the cell surface using 3D reaction-diffusion models of cAMP-PDE interaction in the extracellular space, for a typical microfluidic geometry [16,33] and in space with a point source of cAMP. We use these results to calculate the gradient detection signal-to-noise ratio (SNR) of the receptor response [9,34] and predict how the chemotaxis index is affected by extracellular PDE.

We can gain some intuition about the signal-to-noise ratio (SNR) by considering a linearly increasing cAMP concentration $c(x)$ in 1D, without PDE. Assuming steady state for cAMP to cAMP-receptor binding, each receptor at coordinate x can be thought of as a Bernoulli trial with the probability of being occupied $\rho(x) = c(x)/[c(x) + K_d]$ and unoccupied with probability $1 - \rho(x)$, where K_d is the cAMP to cAMP-receptor binding dissociation constant and represents a concentration at which the $\rho = 0.5$ ([35], §1)

Since the receptor distribution on the cell surface is uniform [41] and $c(x) = c_0 - |\vec{\nabla} c| x$, we can consider each cell half as a single point $x = \mp r_c/2$ (r_c is cell radius, cell is centered at $x = 0$). The distribution of the number of occupied receptors on the front (F) or rear (R) half of the cell follows a Binomial distribution with the average and variance:

$$R_{F,B} = \frac{N}{2}\frac{c_{F,B}}{c_{F,B} + K_d}, \qquad \sigma^2_{R_{F,B}} = \frac{N}{2}\frac{c_{F,B}K_d}{(c_{F,B} + K_d)^2} \quad (1)$$

where $c_{F,B} = c(\mp r_c/2)$ and N is the total number of receptors per cell; here $K_d = 30$ nM, $N = 70\,000$ [42]. The SNR is defined as [9,34] [Fig. 1(a)]

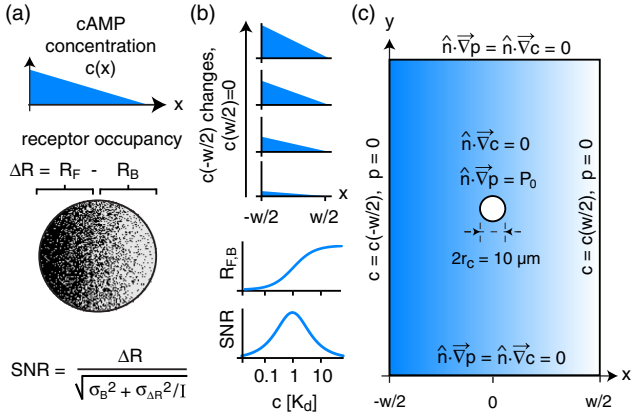

FIG. 1. Signal-to-noise ratio (SNR) and model geometry. (a) The SNR is defined as the receptor occupancy difference between the front half and back half of the cell (signal) divided by the noise consisting of receptor shot noise $\sigma_{\Delta R}$ sampled I times and nonreceptor noise σ_B. (b) When the relative gradient $|\vec{\nabla}c|/c = \text{const}$, the optimal average concentration that maximizes the SNR is $c = K_d$, since the receptor occupancy difference ΔR has a maximum when $c = K_d$ and $\text{SNR} \propto \sqrt{\Delta R}$. (c) Geometry and boundary conditions for 3D numerical simulations; $c = \text{cAMP}$, $p = \text{PDE}$ concentration (not to scale). Constant relative gradient can be set away from the cell (in the bulk), by changing the cAMP concentration on the left boundary $c(-w/2)$, while keeping $c(w/2) = 0$. $w = 1$ mm.

$$\text{SNR} = \frac{\Delta R}{\sqrt{\sigma_B^2 + \sigma_{\Delta R}^2/I}}, \qquad \Delta R = R_F - R_B \tag{2}$$

where ΔR and $\sigma_{\Delta R}^2 = \sigma_{R_F}^2 + \sigma_{R_B}^2$ are the average ("signal") and variance (square of the "noise") of the difference in the number of occupied receptors at the front and back half of the cell, σ_B the nonreceptor noise, and I is the number of statistically independent measurements of the occupied receptors within a sensing period [34].

For shallow gradients, the concentration difference between the cell front and back is small ($r_c|\vec{\nabla}c| \ll K_d$) so the average and variance of the receptor difference are ([35], §2):

$$\Delta R \approx \frac{N}{2}\frac{K_d r_c|\vec{\nabla}c|}{(c_0 + K_d)^2}, \qquad \sigma_{\Delta R}^2 \approx N\frac{c_0 K_d}{(c_0 + K_d)^2}. \tag{3}$$

For fixed relative gradients $|\vec{\nabla}c|/c_0 = \text{const}$: (i) the receptor occupancy $R_{F,B}$ has the steepest increase at $c_0 = K_d$, so $\Delta R \propto dR/dc$ is maximal, and (ii) the receptor noise is proportional to the square root of the signal $\sigma_{\Delta R} \propto \sqrt{\Delta R}$. Then, the SNR is also proportional to the square root of the signal: $\text{SNR} \propto \Delta R/\sqrt{\Delta R} = \sqrt{\Delta R}$ and also maximal at $c_0 = K_d$ [Fig. 1(b)]. Therefore, the optimal average cAMP concentration for gradient sensing without PDE is at exactly K_d when the receptor occupancies are ≈50%.

Fixed PDE secretion flux model.—We first consider a system of two interacting molecules, PDE and cAMP, following Michaelis-Menten kinetics:

$$\text{PDE} + \text{cAMP} \underset{k_{-1}}{\overset{k_1}{\rightleftharpoons}} C_{cp} \overset{k_2}{\rightharpoonup} \text{PDE} + 5'\text{AMP}, \tag{4}$$

where 5′AMP represent the reaction rates, C_{cp} represents the intermediate cAMP-PDE complex, and k_i the product of this reaction (a deactivated signal).

The concentrations of cAMP $c(\vec{r},t)$, PDE $p(\vec{r},t)$, cAMP-PDE complex $C_{cp}(\vec{r},t)$, and the 5′AMP $c'(\vec{r},t)$, are obtained in the standard quasisteady state assumption [43] (intermediate complex is in steady state): $k_1 cp = (k_{-1} + k_2)C_{cp}$, so the two relevant steady-state equations are ([35], §4)

$$D_c\nabla^2 c - \frac{k_2}{K_M}pc = 0, \qquad D_p\nabla^2 p = 0, \tag{5}$$

where D_c and D_p are the diffusion constants of cAMP and PDE, and $K_M \equiv (k_{-1} + k_2)/k_1$. These equations are solved numerically using COMSOL 3.5 (Comsol Inc.) with MATLAB R2011a(The MathWorks, Inc.), for the boundary conditions mimicking typical experiments [16,44,45]; see the results in Fig. 1(c) and Ref. [35], §5. cAMP concentration is varied on the left boundary $c(x = -w/2)$, set to zero on the right boundary $c(x = w/2) = 0$, and the normal cAMP flux is zero everywhere else, including the cell boundary [46]. These boundary conditions result in constant applied relative gradient $|\vec{\nabla}c|_{\text{app}}/c_{0,\text{app}} = 2/w$, where

$$|\vec{\nabla}c|_{\text{app}} = \frac{c(-w/2) - c(w/2)}{w} = \frac{c(-w/2)}{w}, \tag{6}$$

$$c_{0,\text{app}} = \frac{c(-w/2) + c(w/2)}{2} = \frac{c(-w/2)}{2}. \tag{7}$$

For PDE, $p(x = \pm w/2) = 0$ and the normal flux is $P_0 > 0$ at the cell boundary and zero everywhere else. The parameters used in simulations were $K_M = 10\ \mu\text{M}$ [49], $D_c = 444\ \mu\text{m}^2\,\text{s}^{-1}$ [50], $D_p = 70\ \mu\text{m}^2\,\text{s}^{-1}$, $k_2 = 13\,300\ \text{s}^{-1}$ (estimated in Ref. [35], §6), and $r_c = 5\ \mu\text{m}$.

Figure 2(a) shows the SNR, as a function of PDE secretion flux P_0 and cAMP concentration on the left boundary $c(-w/2)$, for the relative gradient $r_c|\vec{\nabla}c|_{\text{app}}/c_{0,\text{app}} = 2r_c/w = 1\%$ across the cell surface. PDE can substantially improve the SNR for a range of P_0 and $c(-w/2)$ values and the improvement is better for large cAMP concentrations. If the midpoint concentration is $\lesssim K_d$ [$c(-w/2) \lesssim 2K_d$], then the SNR can only be decreased by PDE [Fig. 2(b)]. PDE can also broaden the range of cAMP detection by increasing the $c(-w/2)$ range for which $\text{SNR} \geq 1$ [Figs. 2(c), 2(d)].

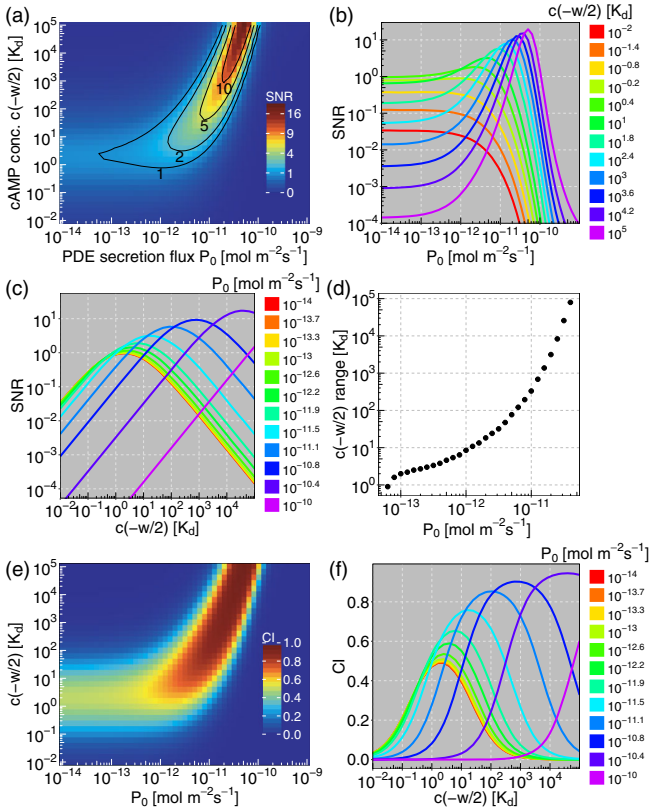

FIG. 2. Fixed PDE secretion flux model with relative gradient on the cell surface of 1%. (a) SNR as a function of PDE secretion flux P_0 and cAMP boundary concentration $c(-w/2)$. The SNR can be substantially improved by PDE for a range of parameters P_0 and $c(-w/2)$. (b) Horizontal slices from (a). PDE can increase the SNR for $c(-w/2) \gtrsim K_d$. (c) Vertical slices from (a). Increasing P_0 shifts the optimal cAMP concentration (maximizing SNR) towards higher values but also broadens the detectable range of cAMP concentrations. The red curve for $P_0 = 10^{-14}$ mol m^{-2} s^{-1} ≈ 0, i.e., matches the SNR in Fig. 1(b) with $c = c(-w/2)/2$. (d) Broadening of curves from (c) is quantified by calculating the range of $c(-w/2)$ for which SNR ≥ 1. (e) Chemotaxis index (CI) calculated as SNR$/$(SNR $+$ 1) ([35], §3). (f) Vertical slices from (e).

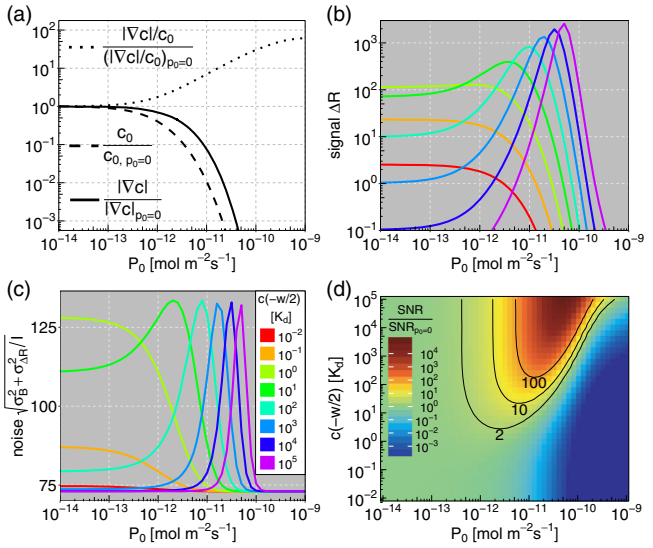

FIG. 3. Signal and noise analysis of the fixed PDE secretion flux model, showing that most of the SNR enhancement results from the increase in signal ΔR. (a) Mean cAMP concentration c_0 and gradient $|\vec{\nabla}c|$ across the cell surface, as a function of PDE secretion flux P_0. When rescaled by their values for $P_0 = 0$, concentration and gradient curves do not depend on $c(-w/2)$. (b) Signal $\Delta R(P_0) \propto |\vec{\nabla}c|/(c_0 + K_d)^2$. Color legend is the same as in (c). (c) Noise $\sqrt{\sigma_B^2 + \sigma_{\Delta R}^2/I}$, with lower limit $\sigma_B = 73$ and upper limit $\sqrt{\sigma_B^2 + N/(4I)} \approx 134$. (d) Ratio of SNR and SNR with $P_0 = 0$.

For parameter values $\sigma_B = 73$ and $I = 1.4$ the measured chemotaxis index (CI) was fit to the empirical equation CI $=$ SNR$/$(SNR $+ 1$) ([35], §3), so the CI also shows both an increase and a wider range for higher P_0 [Figs. 2(e), 2(f)]. The SNR improvement by PDE can also occur when either the absolute gradient $|\vec{\nabla}c|_{\text{app}}$ or the midpoint concentration $c_{0,\text{app}}$ are fixed ([35], §7).

According to Fig. 2, the relevant P_0 range between 10^{-12} and 10^{-10} mol m^{-2} s^{-1}, falls within the rough physiological range estimated here for PDE of 10^{-11} mol m^{-2} s^{-1} ([35], §6.3) and by others for Bar1 of 10^{-12} mol m^{-2} s^{-1} (in yeast) [20].

Next, we analyze how the increase in the SNR is achieved. PDE reduces the average concentration across the cell surface more than it reduces the concentration gradient [Fig. 3(a)], so the signal $\Delta R \propto |\vec{\nabla}c|/(c_0 + K_d)^2$ can be enhanced by multiple orders of magnitude [Fig. 3(b)]. On the other had, the noise has both an upper bound of $\sqrt{\sigma_B^2 + N/(4I)} \approx 134$ at $c_0 = K_d$ [Eq. (3)] and a lower bound at $\sigma_B = 73$ [Fig. 3(c)]. Both follow directly from the definition, Eqs. (2) and (1), and imply that the overall scale of the noise is largely PDE independent. Then, the SNR enhancement comes directly from the signal increase, and can also be increased by multiple orders of magnitude [Fig. 3(d)].

Fixed PDE concentration models.—We consider two models with spatially uniform PDE concentration $p(\vec{r}, t) = p_0$. For the case with the same microfluidic geometry as before but without the cell boundary in the middle, the analytical solution of Eq. (5) is

$$c(x) = c(-w/2)\,\frac{\sinh\left(\frac{w}{2L} - \frac{x}{L}\right)}{\sinh\left(\frac{w}{L}\right)}, \qquad L = \sqrt{\frac{K_M D_c}{k_2 p_0}}, \tag{8}$$

where now a degradation length L appears in the gradient sensed by the cell. At $x = 0$, the cAMP concentration and gradient are

$$|\vec{\nabla}c| = \frac{c(-w/2)}{2L\sinh\left(\frac{w}{2L}\right)}, \qquad c_0 = \frac{c(-w/2)}{2\cosh\left(\frac{w}{2L}\right)}. \tag{9}$$

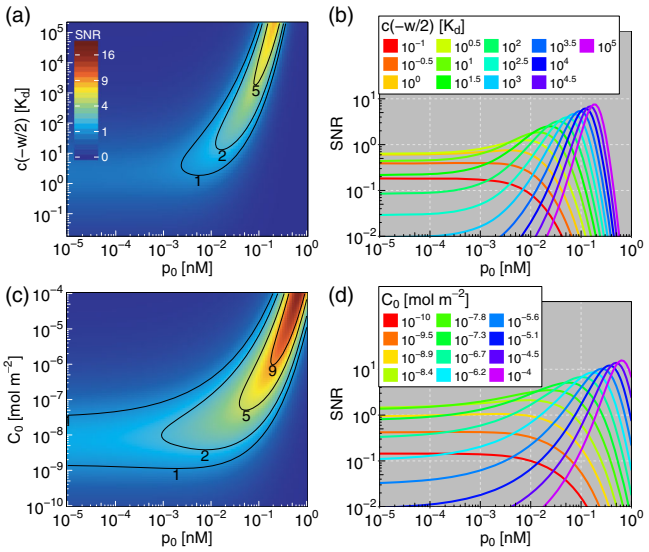

FIG. 4. Analytical solutions for the SNR for a fixed PDE concentration model and a cAMP point source model in 3D, showing a similar enhancement. (a),(b) Microfluidic geometry: SNR as a function of PDE concentration p_0 and cAMP concentration on the left boundary $c(-w/2)$. (c),(d) cAMP point source $C_0\delta(r)$ located at $\vec{r}=0$: SNR as a function of cAMP source strength C_0 and p_0 at a distance $r=225$ μm from the source.

For shallow gradients $r_c|\vec{\nabla}c| \ll K_d$ (well satisfied in this Letter; $\max(r_c|\vec{\nabla}c|/K_d)=5\times10^{-3}$), the SNR [Eq. (2)] is

$$\mathrm{SNR} \approx \frac{NK_d r_c|\vec{\nabla}c|}{2(c_0+K_d)\sqrt{\sigma_B^2(c_0+K_d)^2+Nc_0K_d}}. \quad (10)$$

The SNR is calculated using Eqs. (9) and shows very similar behavior to the fixed PDE secretion flux model [Figs. 4(a), 4(b)], since only the local concentrations in the neighborhood of the cell matter. Intuitively, PDE converts the original relative gradient $\propto r_c/w$ to a new one $\propto r_c/L$ for $L \ll w$ ([35], §8.1). The presence of a cell boundary to a large extent only changes the overall scaling factor ([35], §8.2).

Finally, we consider the case of cAMP emitted by the point source $C_0\delta(r)$. Without PDE, the solution of the steady-state diffusion equation for cAMP concentration $c(\vec{r})$ is equivalent to the electrostatic potential from the point charge at origin, $c(\vec{r}) \sim 1/r$. With uniform PDE, the cAMP concentration becomes $c(r)=C_0e^{-r/L}/r$ ([35], §8.3) and is equivalent to ion screening in classical plasma [51], with Debye length L. PDE increases the relative gradient across the cell from r_c/r to $r_c/r+r_c/L$. For distances below ~0.5 mm from the source, the SNR shows the same enhancement as before [Figs. 4(c), 4(d); Supplemental Material [35], Fig. 8].

Concluding remarks.—In summary, we investigated the effects of extracellular PDE on cAMP gradient sensing in *D. discoideum*. We find that PDE shifts the peak SNR towards higher cAMP concentrations, broadens the range of signal detection, and can also increase the SNR. This contrasts with earlier dimensional analysis estimates [27]. The SNR increase is caused by signal (differential receptor occupancy) increase, while the noise has a PDE-independent upper bound.

Our results qualitatively agree with previous observations of (i) *pdsA* cells responding to a narrower range of cAMP concentrations [22] and (ii) decrease in CI if the cells are starved for longer time periods, and exposed to the same gradient (Fig. 4 in Ref. [45]) since the peak response would shift towards higher cAMP concentrations if the PDE accumulates in the environment. The CI could also be measured for the range of cAMP concentrations for both wild-type and *pdsA* cells and compared to the predictions of our model. The effects discussed here also lead to different predictions between the experiments with static nonflowing gradients where cAMP gradients are affected by secreted PDE [16,44,45] and the experiments with static gradients establish with the flow [11,13,14]. The flow gradient experiments are considered advantageous since the cells are prevented to communicate with each other with cAMP; however, they also completely wash away extracellular PDE ([35], §9). We ignored the effects of receptor internalization and ligand rebinding [52,53] since they lead to small correction here ([35], §10). Note that the SNR enhancement applies in the general case of chemoattractant degradation, but to derive Eq. (5) from Michaelis-Menten kinetics, a slow diffusion limit is needed which is fulfilled here in the relevant PDE range ([35], §11). We also neglected the effects of the PDE inhibitor, expected to be secreted under high PDE levels [54] and would act to increase $K_M \sim$ mM [49] and the role of the noncircular cell shape that may ensure more accurate chemotaxis [55]. Finally, the screening of the chemotactic signal could also result from the secretion of both soluble attractive and repulsive factors, as in angiogenesis [56,57].

We thank the Cornell ACCEL computer lab for access to the COMSOL Multiphysics and MATLAB software, the anonymous referees, and Matteo Mori (UCSD) and Jonathan Desponds (UCSD) for insightful suggestions and comments.

*Present address: Bioinformatics and Structural Biology Program, Sanford Burnham Prebys Medical Discovery Institute, 10901 N. Torrey Pines Road, La Jolla, California 92037, USA.
is246@cornell.edu

[1] K. Swaney, C. Huang, and P. Devreotes, Annu. Rev. Biophys. **39**, 265 (2010).
[2] E. Roussos, J. Condeelis, and A. Patsialou, Nat. Rev. Cancer **11**, 573 (2011).
[3] S. Zigmond, J. Cell Biol. **75**, 606 (1977).
[4] V. Sourjik and N. Wingreen, Curr. Opin. Cell Biol. **24**, 262 (2012).
[5] H. Berg and E. Purcell, Biophys. J. **20**, 193 (1977).

[6] R. Endres and N. S. Wingreen, Proc. Natl. Acad. Sci. U.S.A. **105**, 15749 (2008).
[7] T. Mora and N. S. Wingreen, Phys. Rev. Lett. **104**, 248101 (2010).
[8] B. Hu, W. Chen, W. J. Rappel, and H. Levine, Phys. Rev. Lett. **105**, 048104 (2010).
[9] J.-W. Rappel and H. Levine, Proc. Natl. Acad. Sci. U.S.A. **105**, 19270 (2008).
[10] B. Hu, W. Chen, H. Levine, and J.-W. Rappel, J. Stat. Phys. **142**, 1167 (2011).
[11] D. Fuller, W. Chen, M. Adler, A. Groisman, H. Levine, J.-W. Rappel, and W. Loomis, Proc. Natl. Acad. Sci. U.S.A. **107**, 9656 (2010).
[12] M. Ueda and T. Shibata, Biophys. J. **93**, 11 (2007).
[13] L. Song, S. Nadkarni, H. Bodeker, C. Beta, A. Bae, C. Franck, J.-W. Rappel, W. Loomis, and E. Bodenschatz, Eur. J. Cell Biol. **85**, 981 (2006).
[14] G. Amselem, M. Theves, A. Bae, C. Beta, and E. Bodenschatz, Phys. Rev. Lett. **109**, 108103 (2012).
[15] G. Amselem, M. Theves, A. Bae, E. Bodenschatz, and C. Beta, PLoS One **7**, e37213 (2012).
[16] I. Segota, S. Mong, E. Neidich, A. Rachakonda, C. J. Lussenhop, and C. Franck, J. R. Soc. Interface **10**, 20130606 (2013).
[17] Y. Chang, Science **161**, 57 (1968).
[18] R. Kessin, *Dictyostelium: Evolution and Cell Biology and the Development of Multicellularity* (Cambridge University Press, Cambridge, England, 2001).
[19] N. Barkai, M. Rose, and N. Wingreen, Nature (London) **396**, 422 (1998).
[20] S. Andrews, N. Addy, R. Brent, and A. Arkin, PLoS Comput. Biol. **6**, e1000705 (2010).
[21] M. Jin, B. Errede, M. Behar, W. Mather, S. Nayak, J. Hasty, H. Dohlman, and T. Elston, Sci. Signal. (Online) **4**, ra54 (2011).
[22] G. Garcia, E. Rericha, C. Heger, P. Goldsmith, and C. Parent, Mol. Biol. Cell **20**, 3295 (2009).
[23] L. Tweedy, D. Knecht, G. Mackay, and R. Insall, PLoS Biol. **14**, e1002404 (2016).
[24] R. Shapiro, J. Franke, E. Luna, and R. Kessin, Biochim. Biophys. Acta **758**, 49 (1983).
[25] S. Bader, A. Kortholt, and P. van Haastert, Biochem. J. **402A**, 153 (2007).
[26] S. Orlow, R. Shapiro, J. Franke, and R. Kessin, J. Biol. Chem. **256**, 7620 (1981).
[27] V. Nanjundiah and D. Malchow, J. Cell Sci. **22**, 49 (1976).
[28] E. Palsson and E. Cox, Proc. Natl. Acad. Sci. U.S.A. **93**, 1151 (1996).
[29] E. Palsson, K. Lee, R. Goldstein, J. Franke, R. Kessin, and E. Cox, Proc. Natl. Acad. Sci. U.S.A. **94**, 13719 (1997).
[30] E. Palsson, Biophys. J. **97**, 2388 (2009).
[31] J. Barra, P. Barrand, M. Blondelet, and P. Brachet, MGG, Mol. Gen. Genet. **177**, 607 (1980).
[32] R. Sucgang, C. Weijer, F. Siegert, J. Franke, and R. Kessin, Dev. Biol. **192**, 181 (1997).
[33] S.-Y. Cheng, S. Heilman, M. Wasserman, S. Archer, M. Shulerac, and M. Wu, Lab Chip **7**, 763 (2007).
[34] P. van Haastert and M. Postma, Biophys. J. **93**, 1787 (2007).
[35] See Supplemental Material at http://link.aps.org/supplemental/10.1103/PhysRevLett.119.248101 for derivations, additional results, validity of model assumptions Peclet number analysis, which includes Refs. [36–40].
[36] G. Carta and A. Jungbauer, *Protein Chromatography: Process Development and Scale-Up* (Wiley-WCH, Weinheim, 2010).
[37] M. Tyn and T. Gusek, Biotechnol. Bioeng. **35**, 327 (1990).
[38] R. Yeh, F. Chan, and M. Coukell, Dev. Biol. **66**, 361 (1978).
[39] B. Munson, D. Young, and T. Okiishi, *Fundamentals of Fluid Mechanics* (John Wiley and Sons, New York, 2002).
[40] V. Gurevich and E. Gurevich, Trends Neurosci. **31**, 74 (2008).
[41] T. Jin, N. Zhang, Y. Long, C. Parent, and P. Devreotes, Science **287**, 1034 (2000).
[42] R. Johnson, P. van Haastert, A. Kimmel, C. S. III, B. Jastorff, and P. Devreotes, J. Biol. Chem. **267**, 4600 (1992).
[43] J. Borghans, R. D. Boer, and L. Segel, Bull. Math. Biol. **58**, 43 (1996).
[44] B. Varnum and D. Soll, J. Cell Biol. **99**, 1151 (1984).
[45] P. Fisher, R. Merkl, and G. Gerisch, J. Cell Biol. **108**, 973 (1989).
[46] Zero-normal cAMP flux seems reasonable since the time scale for receptor internalization is 5 min [47] compared to the time scale of receptor dissociation of 1 sec [48], so the binding and unbinding processes are in equilibrium.
[47] A. Serge, S. de Keijzer, F. V. Hemert, M. Hickman, D. Hereld, H. Spaink, T. Schmidt, and B. Snaar-Jagalaska, Integr. Biol. **3**, 675 (2011).
[48] M. Ueda, Y. Sako, T. Tanaka, P. Devreotes, and T. Yanagida, Science **294**, 864 (2001).
[49] R. Kessin, S. Orlow, R. Shapiro, and J. Franke, Proc. Natl. Acad. Sci. U.S.A. **76**, 5450 (1979).
[50] M. Dworkin and K. H. Keller, J. Biol. Chem. **252**, 864 (1977).
[51] L. Landau and E. Lifshitz, *Statistical Physics* (Pergamon Press, New York, 1996), 3rd ed., p. 241.
[52] G. Aquino and R. G. Endres, Phys. Rev. E **81**, 021909 (2010).
[53] R. Endres and N. Wingreen, Prog. Biophys. Molec. Biol. **100**, 33 (2009).
[54] J. Franke and R. Kessin, J. Biol. Chem. **256**, 7628 (1981).
[55] L. Tweedy, B. Meier, J. Stephan, D. Heinrich, and R. Endres, Sci. Rep. **3**, 2606 (2013).
[56] G. Serini, D. Valdembri, S. Zanivan, G. Morterra, C. Burkhardt, F. Caccavari, L. Zammataro, L. Primo, L. Tamagnone, M. Logan, M. Tessier-Lavigne, M. Taniguchi, A. W. Paschel, and F. Bussolino, Nature (London) **424**, 391 (2003).
[57] S. DiTalia, A. Gamba, F. Lamberti, and G. Serini, Phys. Rev. E **73**, 041917 (2006).